



ISTITUTO NAZIONALE DI RICERCA METROLOGICA Repository Istituzionale

Heating of metallic biliary stents during magnetic hyperthermia of patients with pancreatic ductal adenocarcinoma: an in silico study

Original

Heating of metallic biliary stents during magnetic hyperthermia of patients with pancreatic ductal adenocarcinoma: an in silico study / Bottauscio, Oriano; Rubia-Rodríguez, Irene; Arduino, Alessandro; Zilberti, Luca; Chiampi, Mario; Ortega, Daniel. - In: INTERNATIONAL JOURNAL OF HYPERTHERMIA. - ISSN 0265-6736. - 39:1(2022), pp. 1222-1232. [10.1080/02656736.2022.2121863]

Availability:

This version is available at: 11696/74920 since: 2022-11-22T10:50:10Z

Publisher:

TAYLOR & FRANCIS LTD

Published

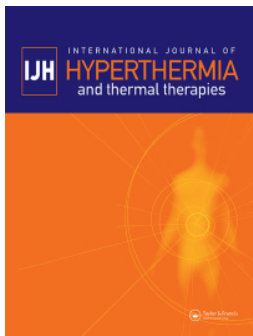
DOI:10.1080/02656736.2022.2121863

Terms of use:

This article is made available under terms and conditions as specified in the corresponding bibliographic description in the repository

Publisher copyright

(Article begins on next page)



Heating of metallic biliary stents during magnetic hyperthermia of patients with pancreatic ductal adenocarcinoma: an *in silico* study

Oriano Bottauscio, Irene Rubia-Rodríguez, Alessandro Arduino, Luca Zilberti, Mario Chiampi & Daniel Ortega

To cite this article: Oriano Bottauscio, Irene Rubia-Rodríguez, Alessandro Arduino, Luca Zilberti, Mario Chiampi & Daniel Ortega (2022) Heating of metallic biliary stents during magnetic hyperthermia of patients with pancreatic ductal adenocarcinoma: an *in silico* study, International Journal of Hyperthermia, 39:1, 1222-1232, DOI: [10.1080/02656736.2022.2121863](https://doi.org/10.1080/02656736.2022.2121863)

To link to this article: <https://doi.org/10.1080/02656736.2022.2121863>



© 2022 The Author(s). Published with license by Taylor & Francis Group, LLC.



Published online: 14 Sep 2022.



Submit your article to this journal [↗](#)



Article views: 873



View related articles [↗](#)









View Crossmark data [↗](#)



Citing articles: 1 View citing articles [↗](#)

Heating of metallic biliary stents during magnetic hyperthermia of patients with pancreatic ductal adenocarcinoma: an *in silico* study

Oriano Bottauscio^a , Irene Rubia-Rodríguez^b , Alessandro Arduino^a , Luca Zilberti^a , Mario Chiampì^a 
and Daniel Ortega^{b,c,d} 

^aIstituto Nazionale di Ricerca Metrologica (INRIM), Turin, Italy; ^bIMDEA Nanoscience, Madrid, Spain; ^cCondensed Matter Physics Department, University of Cádiz, Cádiz, Spain; ^dInstitute of Research and Innovation in Biomedical Sciences of Cádiz (INIBICA), University of Cádiz, Cádiz, Spain

ABSTRACT

Objective: To investigate the eddy current heating that occurs in metallic biliary stents during magnetic hyperthermia treatments and to assess whether these implants should continue to be an exclusion criterion for potential patients.

Methods: Computer simulations were run on stent heating during the hyperthermia treatment of local pancreatic tumors (5–15 mT fields at 300 kHz for 30 min), considering factors such as wire diameter, type of stent alloy, and field orientation. Maxwell's equations were solved numerically in a bile duct model, including the secondary field produced by the stents. The heat exchange problem was solved through a modified version of the Pennes' bioheat equation assuming a temperature dependency of blood perfusion and metabolic heat.

Results: The choice of alloy has a large impact on the stent heating, preferring those having a lower electrical conductivity. Only for low field intensities (5 mT) and for some of the bile duct tissue layers the produced heating can be considered safe. The orientation of the applied field with respect to the stent wires can give rise to the onset of regions with different heating levels depending on the shape that the stent has finally adopted according to the body's posture. Bile helps to partially dissipate the heat that is generated in the lumen of the bile duct, but not at a sufficient rate.

Conclusion: The safety of patients with pancreatic cancer wearing metallic biliary stents during magnetic hyperthermia treatments cannot be fully assured under the most common treatment parameters.

ARTICLE HISTORY

Received 31 May 2022
Revised 23 August 2022
Accepted 2 September 2022

KEYWORDS

Biliary stent; magnetic hyperthermia; eddy currents; electromagnetic dosimetry; *in silico*

1. Introduction

Metallic implants undergo eddy current heating under alternating magnetic fields (AMFs), which usually limit the extent to which implanted patients qualify for magnetic hyperthermia treatments to the point of exclusion [1,2]. The proportion of this patient subpopulation is significant, above all considering that older patients are more frequently diagnosed with cancer, and also that palliative treatment for various types of cancer involves the use of implants. For example, from 70 to 90% of pancreatic cancer patients frequently suffer from bile duct blockage by the time they are diagnosed. The most common palliative treatments in those cases entail either surgical by-passing or endoscopic stenting, being the latter the preferred option [3]. Biliary stents relieve the distal biliary obstruction due to invasive pancreatic adenocarcinomas, facilitating the drainage of bile into the digestive tract. There are two main types, namely plastic and self-expandable metallic biliary stents (MBS). MBSs have the ability of expanding to a much larger diameter than that of the endoscope – thus increasing the associated patency, i.e.,

their capacity of remaining open and unobstructed. This fact and a better durability are advantages of MBSs over their plastic counterparts [4]. Nevertheless, they heat up under alternating magnetic fields (AMFs), which increases the risk of implanted patients to suffer from injuries or even burns when submitted to magnetic hyperthermia treatments or any others implying the use of AMFs. The application of pulsed AMFs instead of a continuous application during treatment has been recently proposed as a means to mitigate thermal stress in healthy tissue [5,6]. While the resulting *in vitro* and *in vivo* data are promising, the improvement brought about through the use of pulsed fields on the collateral heating of metallic prostheses remains to be studied. In the meantime, passive implantation remains a reason for direct exclusion for prospective patients in magnetic hyperthermia treatments [1,7]. On the basis of a previous electromagnetic model to assess eddy current heating of prostheses in magnetic hyperthermia [8], here we present an original model to account for the peculiarities of MBS under AMFs. Applying this model to a virtual phantom of the bile duct will allow to simulate non-conventional positioning of

MBS, which is the usual case given the complex orientation of the latter in the pancreatic region and the flexibility of MBS. The influence of the stent wire gauge, presence of bile into the duct, stent material, or field intensity and orientation with respect to the stent major dimension is established. Finally, we discuss the implications of the collateral heating of MBS on both the treatment planning and its performance in pancreatic cancer patients under different conditions complying with the relevant safety rules [9,10].

2. Materials and methods

The bile duct is a tube that connects the gallbladder and the duodenum in the small intestine to transport there the bile, where it performs essential tasks for food digestion [11]. This tube is part of the biliary tree, which starts in the liver. The part of this tree that comes out from the gallbladder is called cystic duct which is joined along with the common hepatic duct into the common bile duct. This goes through the pancreas and joins with the pancreatic duct, ending up in the ampulla of Vater in the duodenum. It is very common to see that the tumor blocks this path in pancreatic ductal adenocarcinoma (PDAC) patients, avoiding the bile to reach the small intestine [12]. This is clinically shown as jaundice (yellow colored skin) due to the accumulation of bilirubin in the blood, which is a component of the bile.

The bile duct is mainly composed of three layers of tissue. The innermost part is the mucosa layer, joined by the submucosa layer to the outermost layer, which is the *muscularis propria* [13]. The thickness of these three layers varies along the path of the duct, but, for simplicity, these have been considered with homogeneous thickness throughout the entire length of the virtual phantom of the bile duct we have built for this study.

The human model used for the simulations was Duke from IT'IS Foundation virtual family [14,15]. This is a healthy human phantom, therefore, no tumors are present in the model. Also, it lacks from the bile duct geometry, so it was entirely modeled in Blender, an open-source explicit modeling tool [16] following CT scans provided by the Gastrointestinal Tumors Service of the Medical Oncology Service at the University Hospital of Vall d'Hebron for reference. The models of the pancreas, liver, gallbladder, stomach, intestines, and big blood vessels from Duke model were used to limit the space through which the bile duct can run. For this matter, a hollow cylinder was deformed following a Bezier curve that draws the path of the bile duct. This model represents the inner layer of the physiological tube which was duplicated to obtain the rest of tissue layer phantoms

by increasing their diameters. The resulting thickness for each layer are 0.33, 0.23, and 0.35 mm, from inner to the outermost, following the thicknesses found in the literature for each layer [13,17–19]. The inner diameter of the duct goes from 5 to 7 mm.

For the stent representation, the open stent model from [20] was used. They developed two different versions of the stent, one that is completely expanded (or opened) and a second one which corresponds to the closed stent. The first one was deformed in Blender to mimic a stent that is not completely expanded due to the pressure that the PDAC produces on the bile duct. The stent length is 13.6 mm, while its diameter ranges from 6 mm to 7.5 mm.

For the human tissues included in the Duke model, the physical properties assigned to each of them were the ones included in the IT'IS Foundation database [21]. For the case of the bile duct, the properties corresponding to each layer of tissue were found in [22], except for the values for the connective tissue which are also available in the IT'IS Foundation Database [21]. Some of the most common stent alloys in the market have been considered, namely Elgiloy® (Co–Cr–Ni–Fe–Mo–Mn), and both the martensitic and austenitic phases of nitinol (Ni–Ti). The physical properties adopted for this study are summarized in Table 1. Apart from thermo-regulation effects (involving the metabolic heat and the blood perfusion in tissues), in the simulations all physical parameters of both the biological tissues and the stents have been considered as independent of temperature.

The simulations were performed in two steps. In the first one, the electromagnetic phenomena induced within the metallic stent model and the surrounding tissues are evaluated by means of an own electromagnetic software derived from the one used in Ref. [8]. This software solves the Maxwell equation in the frequency domain formulated in terms of an electric scalar potential ϕ and a magnetic vector potential \mathbf{A}_s that is linked to the field sources. The domain is constituted by the conductive tissues, discretized in voxels, and the differential equations are numerically solved by means of a finite element approach. The chosen voxel size in all simulations was 0.2 mm, which represents a good tradeoff between accuracy and computational time. Dirichlet boundary conditions are applied at the domain boundary, assuming that the induced currents are confined within the considered domain. This approach is applicable in the absence of ferromagnetic materials, which is the case for the metallic alloy considered in this analysis. One of the most complex aspects to deal with in this study is the reduced wire gauge of the MBS. The discretization of the thin metallic wires directly within the voxel dataset of the human

Table 1. Relevant physical properties of the bile duct tissues and the stent alloy.

Tissue	Muscularis propria	Submucosa layer	Mucosa layer	Connective tissue	Bile	Nitinol (austenite)	Nitinol (martensite)	Elgiloy®
Electrical conductivity (S/m)	0.202	0.251	0.511	0.39	1.4	10^6	1.25×10^6	10^6
Density (kg/m ³)	1090	1027	1088	1027	928	6450	6450	8300
Heat capacity (J/(kg·K))	3421	2372	3690	2372	4037	837	837	430
Thermal conductivity (W/(m·K))	0.49	0.39	0.53	0.39	0.58	18	8.6	12.5
Heat transfer rate (ml/(min·kg))	37	37	460	37	0	–	–	–
Heat generation rate (W/kg)	0.91	0.58	7.13	0.58	0	–	–	–
Reference	[22]	[22]	[22]	[21]	[21]	[23]	[23]	[24]

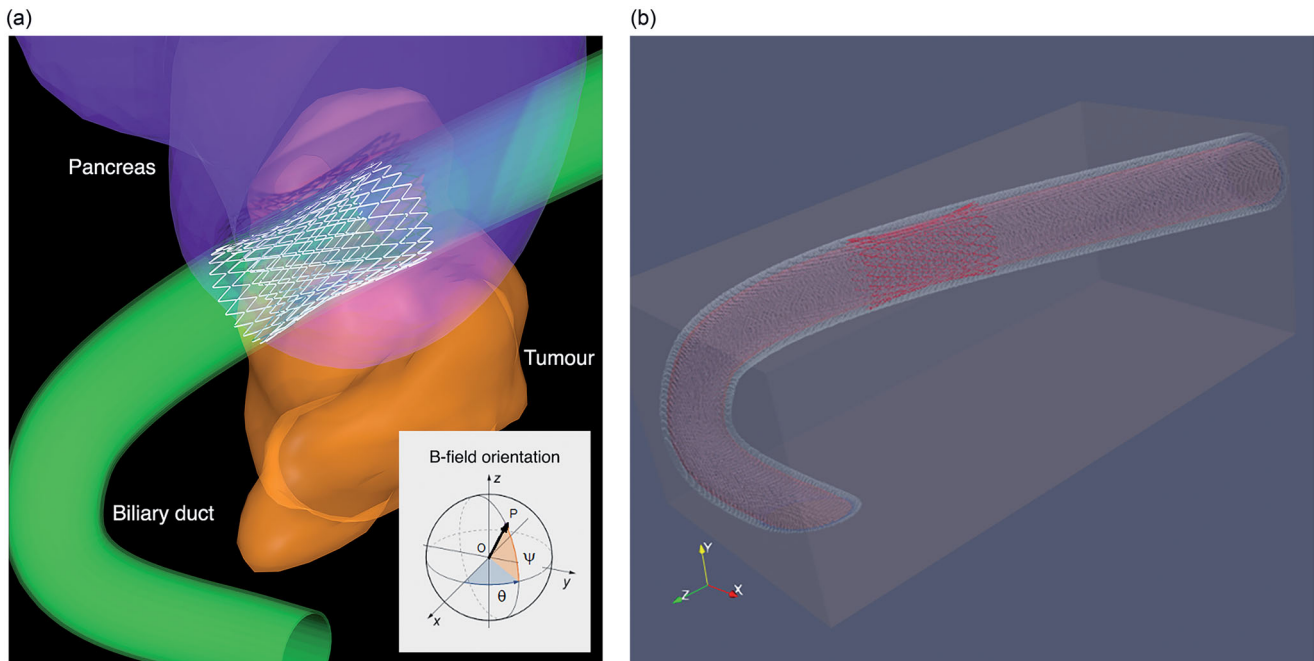


Figure 1. (a) Model of the bile duct (green) and tumor along with the detail of the 1D structure of the metallic stent. The angles identifying the stent axis are: $\psi = 72.5^\circ$ and $\theta = 0^\circ$. The orientation reference for admissible field directions is indicated in the inset. (b) Full computational model domain.

anatomy would be critical, because, in order to get a good geometrical representation of the wires themselves (reducing staircase errors [25] that affects the computation of the induced eddy currents), an extremely fine resolution would be required [25]. To avoid this problem, the filamentary wires of the MBS are modeled as one-dimensional elements constituting an electric grid, where each branch of the circuit is described by an electric circuit element with its own electrical resistance. Figure 1(a) shows the model of the considered structure with the duct and the grid representing the MBS embedded in the correct anatomical position.

In this electric circuit, currents (unknowns) induced in all the branches by the interaction with the magnetic field generated by the source are evaluated, following an approach that is an evolution of the one adopted in [26], starting from the main concepts adopted in the same reference. The induced electromotive forces in the circuit branches are accounted for by line integrals of the magnetic vector potential \mathbf{A}_s , determining consequently the linked magnetic fluxes. This approach assumes that the current flowing within the wires is confined in the metallic elements; this assumption is reasonable, considering the ratio between the electrical conductivity of the metal and the one of the tissues. The reaction field generated by the induced currents is taken into account, being significant at the increase of the frequency. This is done by computing the magnetic vector potential \mathbf{A}_r caused by the current flowing into the circuit branches. This term is summed to the magnetic vector potential \mathbf{A}_s of the sources to evaluate the electric scalar potential ϕ in the conductive tissues. The essential governing equations for the electromagnetic problem are summarized in the Appendix, while more details of the computational aspects related to the adopted approach can be found in [27].

After solving the electric circuit associated with the stent, the power dissipated in each wire is computed and distributed into the voxels of the anatomical body crossed by the wire. At the same time, the current density induced in the native tissues is determined through the solver adopted in Ref. [8], including both the source and the reaction field due to the currents induced in the MBS.

Once the power dissipated into the stent and the surrounding tissues has been evaluated, it is possible to proceed with the computation of the time evolution of the temperature increase (ΔT) in the relevant tissues for the entire exposure time. The bioheat equation is solved adopting the same approach used in Ref. [8], which includes thermoregulation effects.

The computational domain (Figure 1(b)) was in principle defined by a trial-and-error procedure to guarantee that the temperature increase at the domain boundary was nearly null after 1800 s. This is due to the fact that the stent heating is extremely localized; heat diffusion toward the surrounding tissues is also contained by perfusion and thermoregulation effects. Under this assumption, Dirichlet boundary conditions are assumed at the domain boundary ($\Delta T = 0$), assuming that the domain is sufficiently large to guarantee that the heat does not diffuse toward the external region at the end of the exposure time. This condition is verified at the end of each simulation. In the initial state (before exposure to the magnetic field sources), the temperature increase is assumed to be null, which means the tissues are at the resting state. The local temperature can be finally determined as the sum of the local value of ΔT and the local value of the temperature at rest (T_0), that is, before exposure.

Simulations have been performed assuming the patients have undergone pre-operative fasting, but for illustrative

purposes, two conditions have been considered when solving the heat exchange problem: (a) a void bile duct (which could be the case if a severe stricture or stone obstruction is present), hence the internal channel has been assumed to be filled with air, (b) a bile duct completely full of bile in motionless conditions. Since bile flow in humans is about 17 $\mu\text{L/g}$ liver/h amounting to a total of 750 ml a day [28,29], no noticeable changes in heat transfer were expected when considering the bile flow itself. In previous reference clinical studies, Johannsen et al. [7,30] reported on therapy sessions entailing the application of AMFs with a fixed frequency of 100 kHz and a variable field intensity within the 3.1–19 mT range, starting from the lowest end and then gradually increasing as tolerated by each patient. Maier-Hauff et al. [2] used the same conditions, with adjustments as deemed necessary during the sessions. All these trials were conducted following a continuous duty cycle of 60 min, unlike the ongoing NoCanTher clinical study [31], where AMFs with a 5 mT intensity at 300 kHz are used, following a pulsed duty cycle amounting to 10 min on over 15 min treatment. Thus, the chosen conditions in our simulations—magnetic flux density in the duct region ranging from 5 mT to 15 mT at a fixed frequency of 300 kHz, and 30 min continuous duty cycle—are therefore representative of a medium-to-worst-case scenario of relatively large field intensity and frequency, and continuous heating. Representing the most commonly used average dimensions of MBSs [32], the wire diameter of the stent was assumed to be within the 0.1–0.4 mm range. Most of the simulations have been performed using a diameter of 0.3 mm. The impact of the wire diameter on the col-lateral MBS heating is dealt with in Section 3.3. Finally, in relation to the electrical contact between the individual wires, MBSs have been considered as perfectly braided with no electrical contact losses.

3. Results and discussion

Due to the geometry of MBSs, the heating is localized in the surrounding tissues and ΔT rapidly decreases, moving away from the stent region. An example of the spatial distribution of ΔT induced by the magnetic field oriented along the direction that produces the highest temperature increase (it will be later denoted as B_{max}) is plotted in Figure 2 for the full bile duct.

The interpretation of the obtained results in the following sections depends on where the threshold for thermal damage—either reversible or irreversible—is set. Temperatures as low as 42 °C can already induce some thermal damage, but it would require very long exposure times, and the response would be different depending on the type of tissue. As can be seen from the comparison of the results obtained from several dedicated models for blood perfused skin [33], the rate of thermal damage roughly increases three orders of magnitudes every 10 °C in the 40–100 °C temperature range [34]. Whereas this noticeable increase does not translate into a relevant thermal damage at low tissue temperatures, it does within 50–60 °C. It has been demonstrated through ablation studies that instant irreversible thermal damage in

the liver occurs at 73.4 °C [35]. In fact, the calculated exposure times required to induce first, second, and third degree burns in blood perfused tissues reveal that, on average, it takes around 24 h to induce a first degree one at 40 °C, about one second or less at 60 °C, and almost no time at 80 °C [34]. These findings may not directly apply to the bile duct and adjacent tissues, but they constitute a first precedent given the very few data on thermal damage of these tissues. The outcomes from *in vivo* studies on irreversible electroporation (IRE) in pigs, where the temperature of the typically employed electrodes reaches values between 44 °C and 50 °C, find no harm induced neither in liver blood vessels nor in the bile ducts [36]. Similarly, several clinical studies on IRE of liver tumors [37,38] confirmed that bile ducts close to the IRE ablation were not significantly affected. The important lack of data on thermal damage of bile duct makes it necessary to resort to references focused on other tissues that may have similar structure and properties, for example blood vessels. A study on ultrasound heating shows that even small vessels in the blood brain barrier can withstand temperatures around 48–49 °C for relatively short exposure times of several minutes, but there is a 50% probability of inducing tissue damage in the form of vascular occlusion and hemorrhage [39]. Finally, it is convenient to recall that 43 °C is chosen for mild hyperthermia treatments, whereas 50 °C is considered ablation.

Considering the facts above and given the moderate perfusion of the bile duct and the bile flow rate, 46 °C has been taken as the threshold for tissue thermal damage in the coming results subsections.

3.1. Effect of the field orientation

The orientation of the incident magnetic field plays a role in determining the induced phenomena in the stent as a consequence of the different coupling. Since the relative position between stent and source cannot be determined *a priori* (depending on the treatment procedure), many possible relative orientations have been explored to find the variability on the resulting heating and determining the worst operative scenario. MBSs also fold to a degree that is difficult to predict because it depends on the internal position of tumors and surrounding organs, which complicates treatment planning. This preliminary analysis was performed assuming a wire diameter of 0.3 mm, and a field amplitude corresponding to 10 mT in the stent region under the two limit scenarios of an empty and a full bile duct.

The set of admissible field directions coincides with a hemisphere (Figure 1), where each direction is identified by a segment OP from the center of the hemisphere (O) to a point on the hemisphere (P). The hemisphere is described in spherical coordinates, in which the latitude ψ is the angle between OP and its projection on the plane $z=0$, whilst the longitude θ is the angle between the projection of OP in the plane $z=0$ and the x -axis. Figure 3 shows the maps of the total power dissipated into the stent, the maximum power density within the stent and the corresponding maximum ΔT reached in the surrounding tissues after 30 min of exposure.

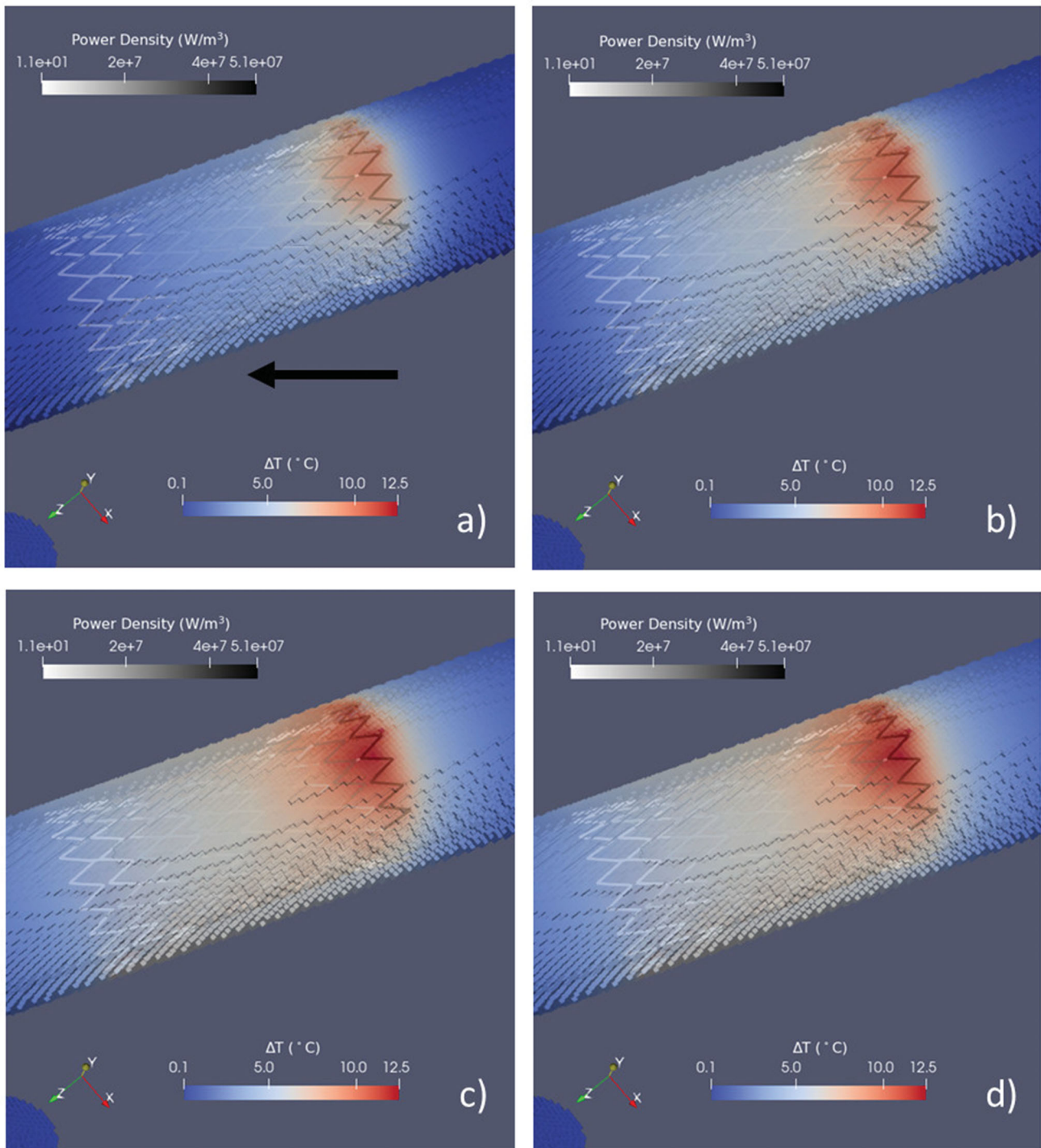


Figure 2. Time evolution of the spatial distribution of ΔT during the exposure to the B_{\max} field orientation upon exposure after 10 s (a), 60 s (b), 360 s (c), and 1800 s (d). The field amplitude is 5 mT, and the wire diameter is 0.3 mm. The maps refer to the duct full of bile. Two different color maps are used to represent the temperature increase in the tissues and the power density in the stent wires. The black arrow in (a) shows the direction of B_{\max} ($\psi = 52^\circ$ and $\theta = 130^\circ$).

The ratio between the maximum ΔT obtained with the field directions that maximize and minimize the heating of the stent is found to be around 1.75. Both with and without the bile in the duct, the maximum heating is obtained for a field orientation corresponding to $\psi = 52^\circ$ and $\theta = 130^\circ$ (position identified as B_{\max}), which is off the MBS major axis.

It is worth noting that neither the maximum total power nor the maximum peak power density is associated with the direction B_{\max} at which the temperature increase is maximum.

3.2. Effect of the duct content

During fasting—which is the reference state for patients under treatment—about 75% of the bile is diverted to the gallbladder, whereas around 25% flows directly to the bile duct toward the duodenum [40]. Thus, considering an empty bile duct would not be entirely realistic in a stented patient, as this could be indicative of gallbladder sludge or stones [41]. Additionally, the gallbladder absorbs a large proportion

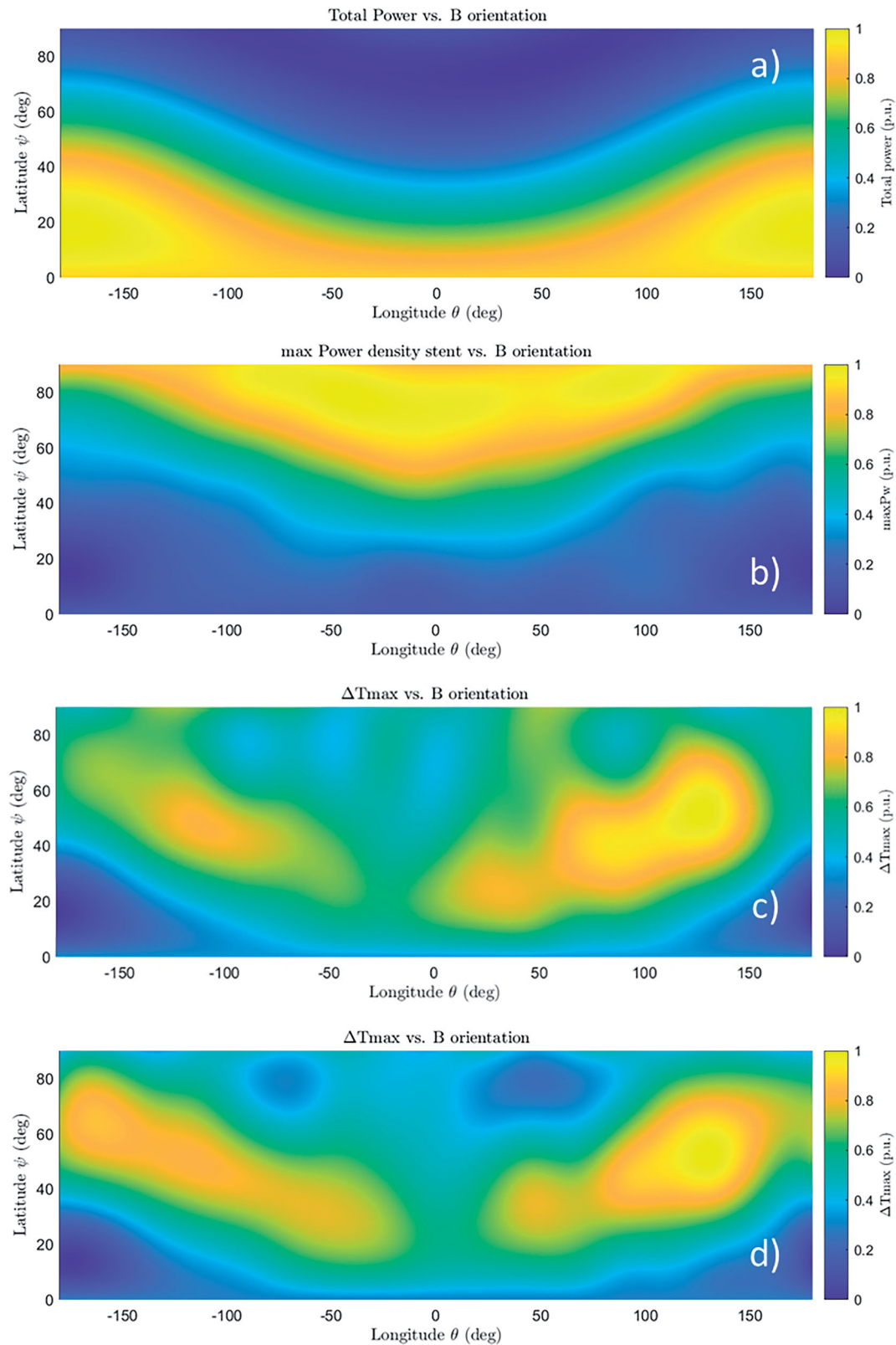


Figure 3. Influence of the magnetic field orientation on the power deposition in the stent and the consequent tissue heating after 30 min of exposure. From the upper plot to the bottom: (a) total power dissipated into the stent, (b) maximum power density in the stent, (c) corresponding maximum temperature increase (ΔT_{\max}) in tissues for an empty duct, (d) corresponding ΔT_{\max} in tissues for a duct full of bile. All the results, obtained at 300 kHz, are reported in p.u. values, where the values of zero correspond to the minimum of the physical quantity, while the value of one correspond to the maximum of the physical quantity.

of water from the bile, resulting in an increased concentration of bile salts and perhaps introducing significant changes in its physical properties. A different heating is obtained

when the bile duct is considered to be empty or full, due to the different thermal properties of the bile with respect to the air (e.g., bile has about twenty times the thermal

conductivity of air). This effect was studied considering four different field orientations (along the three Cartesian axes and along the direction producing the maximum heating, B_{\max}), assuming an amplitude of 10 mT and a wire diameter of 0.3 mm. Results are summarized in Table 2, where the ΔT_{\max} reached in the different tissues is reported for the different cases. The largest variations in the calculated ΔT_{\max} values between the empty or full bile duct cases are seen in the mucosa and submucosa layers—primarily in the first one—which are the closest substructures to the lumen. This observation is consistent with the physical properties of the media involved: it is more difficult to heat or cool down the bile because it has a heat capacity that is four times that of the air, however, bile can move heat much quicker than air by virtue of its almost twenty times higher thermal conductivity of air. Nevertheless, the heat load produced by the MBS during the treatment can be dissipated down to reasonable values so that the possible thermal damage to the bile duct could be acceptable.

3.3. Effect of the wire size

The size of the wire has a great impact on the power dissipated in the stent. Indeed, the wire electrical resistance varies, limiting the induced current circulation—and, in principle, the dissipated power—when the diameter is reduced. In Table 3, ΔT_{\max} values after a 30-min exposure obtained for the different tissues are reported considering both full and empty duct cases, and the magnetic field oriented along B_{\max} .

From the theoretical point of view, a non-monotonic behavior of the power deposited within the stent with respect to the wire diameter is possible (due to the reaction field produced by the induced currents themselves). However, for the realistic geometry and wire diameters here considered, such a power exhibits a strictly monotonic trend.

This aspect is crucial in treatment planning, as this in itself may imply moving from a wire diameter that entails

relatively tolerable ΔT to one that may induce irreversible thermal damages even at moderate or low field strengths. For example, going from a wire diameter of 0.1 mm to a 0.2 mm one leads to a still tolerable ΔT_{\max} value at 5 mT (Table 3), whereas doing the same at 10 mT could cause irreversible damages to the patient. This effect is even more dramatic for larger wire diameters. The outcomes of these simulations tell us that the wire diameter may not preclude an MBS-bearing patient to undergo magnetic hyperthermia therapy as there are many commercial MBS models with diameters between 0.1 and 0.2 mm that are used to alleviate strictures due to PDAC tumors. Thus, the only limiting parameter would be the field amplitude, or the combination of field frequency and amplitude. ΔT_{\max} values for an empty duct show the evident worsening of the heating effect in the case of an obstruction precluding the bile flow, inducing temperature differences close to 20 °C in the mucosa and submucosa tissues for some of the reported field intensities.

A further insight into the implications of the wire size can be obtained by calculating the amount of tissue mass where the produced heating exceeds a certain threshold value of ΔT_{\max} for each tissue. Table 4 compiles the calculated results for a threshold ΔT_{\max} (designated as ΔT_{\lim}) of 80%. The mass amount over ΔT_{\lim} decreases as the ΔT_{\max} increases in each tissue layer of the duct, contrarily to what could be initially expected. This trend reflects the magnitude of the compensation mechanism, in terms of thermoregulation, that occurs depending on the particular ΔT_{\max} . Through a certain distance within a given tissue volume, high ΔT_{\max} values will entail a quicker temperature decrease due to a larger associated perfusion coefficient, therefore the amount of mass with a $\Delta T_{\max} > \Delta T_{\lim}$ will be lower in percentage.

3.4. Effect of the field intensity

The intensity of the applied field does not affect the heating in a straightforward manner due to the thermoregulation

Table 2. ΔT_{\max} (°C) after 30 min of exposure to a 10 mT field calculated for the tissues that make up the bile duct, with or without bile in the duct.

Direction	Mucosa Layer		Submucosa layer		Muscularis propria		Connective tissue	
	Duct full of bile	Empty duct	Duct full of bile	Empty duct	Duct full of bile	Empty duct	Duct full of bile	Empty duct
x	43.0	58.2	43.6	47.8	42.5	45.5	42.2	44.4
y	44.9	58.8	40.2	44.1	33.1	35.3	25.8	30.7
z	40.1	50.0	39.2	44.1	35.8	39.3	28.9	34.1
B_{\max}	55.6	72.1	57.3	70.4	53.3	64.3	45.5	59.3

As indicated before, B_{\max} is the field direction for which a maximum heat is obtained.

Table 3. ΔT_{\max} (°C) after 30 min of exposure.

Field amplitude (mT)	Wire diameter (mm)	Mucosa layer	Submucosa layer	Muscularis propria	Connective tissue
5	0.1	2.91 (3.76)	2.89 (3.60)	2.70 (3.39)	2.58 (3.34)
	0.2	7.53 (8.73)	7.83 (8.76)	7.44 (8.19)	6.47 (7.43)
	0.3	14.5 (17.9)	15.0 (17.8)	14.1 (16.4)	12.1 (14.9)
	0.4	24.8 (31.2)	25.7 (30.8)	24.0 (28.2)	20.4 (25.8)
10	0.1	7.54 (8.73)	7.83 (8.76)	7.44 (8.19)	6.46 (7.43)
	0.2	25.0 (31.5)	25.9 (31.1)	24.2 (28.5)	20.6 (26.0)
	0.3	55.6 (72.1)	57.3 (70.4)	53.3 (64.3)	45.4 (59.3)
	0.4	>100	>100	>100	>100

The field is oriented along the B_{\max} direction, with amplitudes equal to 5 mT and 10 mT. For comparison purposes, the calculated ΔT_{\max} values considering an empty duct are indicated in brackets. Values are not reported for the cases where ΔT_{\max} exceeds 100 °C.

Table 4. Amount of tissue mass (milligrams) of a given tissue where the heating exceeds 80% of the maximum temperature increase ΔT_{\max} found in each tissue ($\Delta T_{\lim} = 0.8 \cdot \Delta T_{\max}$).

B (mT)	Wire diameter (mm)	Mucosa layer		Submucosa layer		Muscularis propria		Connective tissue	
		ΔT_{\max} (°C)	Mass (mg)	ΔT_{\max} (°C)	Mass (mg)	ΔT_{\max} (°C)	Mass (mg)	ΔT_{\max} (°C)	Mass (mg)
5	0.1	2.91	3.93	2.89	2.56	2.70	6.83	2.58	8.27
	0.2	7.53	1.93	7.83	1.08	7.44	2.21	6.47	4.98
	0.3	14.5	0.88	15.0	0.64	14.13	1.40	12.05	2.47
	0.4	24.8	0.71	25.7	0.58	24.0	1.33	20.43	2.25
10	0.1	7.54	1.93	7.83	1.08	7.44	2.21	6.47	4.96
	0.2	25.0	0.71	25.9	0.58	24.2	1.33	20.6	2.26
	0.3	55.6	0.69	57.3	0.55	53.3	1.26	45.5	2.19
	0.4	–	–	–	–	–	–	–	–

Values are not reported for the cases where ΔT_{\max} exceeds 100 °C. For each tissue, the amount of mass was computed extracting the number of voxels whose temperature increase is higher than ΔT_{\lim} ; the number of voxels defines the volume that is multiplied by the tissue mass density to get the total mass.

Table 5. Calculated ΔT_{\max} (°C) for each of the bile duct tissue layers after 30 min exposure to different field intensities along four different orientations.

B (mT)	Direction	Stent power (W)	Mucosa layer	Submucosa layer	Muscularis propria	Connective tissue
5	x	0.548	11.6	11.9	11.6	11.7
	y	0.540	12.1	11.0	9.5	7.5
	z	0.614	10.9	10.8	10.0	8.0
	B_{\max}	0.586	14.5	15.0	14.1	12.1
10	x	2.191	43.0	43.6	42.5	42.2
	y	2.159	44.9	40.2	33.1	25.8
	z	2.454	40.1	39.2	35.8	28.9
	B_{\max}	2.342	55.6	57.3	53.3	45.5
15	x	4.930	>100	>100	>100	>100
	y	4.858	>100	>100	>100	>100
	z	5.522	95.5	90.9	82.4	71.0
	B_{\max}	5.270	>100	>100	>100	>100

The duct is full of bile.

Table 6. Amount of tissue mass (grams) where the heating exceeds 3 °C, 6 °C, and 9 °C.

ΔT_{\max} (°C)	B (mT)	Mucosa layer		Submucosa layer		Muscularis propria		Connective tissue	
3	5	0.122	22.1 %	0.080	21.6 %	0.134	21.2 %	1.210	2.7 %
	10	0.175	31.6 %	0.116	31.2 %	0.197	30.9 %	4.472	9.8 %
	15	–	–	–	–	–	–	–	–
6	5	0.068	12.3 %	0.043	11.6 %	0.063	9.9 %	0.077	0.17 %
	10	0.126	22.8 %	0.083	22.4 %	0.140	22.1 %	1.475	3.2 %
	15	–	–	–	–	–	–	–	–
9	5	0.0085	1.54 %	0.0061	1.65 %	0.0076	1.19 %	0.0042	0.01 %
	10	0.107	19.4 %	0.070	18.9 %	0.118	18.5 %	0.771	1.70 %
	15	–	–	–	–	–	–	–	–

The percentage with respect to the entire tissue mass in the considered duct tract is also reported. Values are not reported for cases where ΔT_{\max} exceeds 100 °C. For each tissue, the amount of mass was computed extracting the number of voxels whose ΔT_{\max} exceeds the given 3 °C, 6 °C, and 9 °C thresholds; the number of voxels defines the volume that is multiplied by the tissue mass density to obtain the sought total mass.

effects that take place in the tissues. This phenomenon was investigated by varying the field amplitude within the 5–15 mT range. Results are collected in Table 5, where the ΔT_{\max} experienced in the different tissues after 30 min of exposure are reported for different field intensities and four field orientations considering a wire diameter of 0.3 mm. With very rare exceptions, an average MBS within the studied field range would produce a potentially harmful—extremely harmful in many cases—heat load in a portion of the bile duct tissue layers during the typical treatment time. The quadratic scaling of the deposited power with the field intensity makes ΔT_{\max} much more pronounced for increasing intensities, reaching instantaneous tissue ablation extremes in all the field orientations under 15 mT.

To have a quantitative estimation of the tissue volume around the stent involved in the heating, for each exposure scenario, the amount of tissue mass which exceeds the threshold of 3 °C and 6 °C for ΔT after 30 min was evaluated. The choice of these thresholds has been made so they

roughly cover temperature values that represent the typical target one for mild hyperthermia (43 °C) and another below for reference (40 °C). Results are collected in Table 6.

3.5. Dependence of heating on alloy type

Table 7 shows the influence of the stent material (Elgiloy and Nitinol alloys) on the attained ΔT_{\max} at the different tissue layers of the bile duct upon MBS heating during a 30-min magnetic hyperthermia session. ΔT_{\max} values obtained for the Ti-6Al-4V alloy, which is widely used in other prostheses due to its excellent corrosion resistance, are shown to illustrate the case of a material with a considerably lower electrical conductivity compared to the others. Elgiloy leads to the same results as with Nitinol (under its austenitic phase) because they have the same electrical conductivity. The different thermal conductivity of these alloys does not play any role for two reasons: (a) their thermal conductivity values are in any case higher with respect

Table 7. ΔT_{\max} (°C) after 30 min of exposure.

Alloy type	Overall max	Mucosa layer	Submucosa layer	Muscularis propria	Connective tissue
Nitinol (Austenite)	57.3 (>100)	55.6 (72.1)	57.3 (70.4)	53.3 (64.3)	45.4 (59.3)
Nitinol (Martensite)	71.6 (>100)	69.7 (>100)	71.6 (>100)	66.6 (>100)	57.0 (>100)
Elgiloy	57.3 (>100)	55.6 (72.1)	57.3 (70.4)	53.3 (64.3)	45.4 (59.3)
Ti-6Al-4V (*)	32.3 (>100)	31.1 (39.1)	32.2 (39.4)	29.5 (35.1)	25.6 (32.5)

The field is oriented along B_{\max} direction and its amplitude is equal to 10 mT. The representative wire diameter is 0.3 mm in all the cases. The values obtained considering an empty bile duct are shown in brackets for comparison.

(*) Electrical conductivity = $0.56 \cdot 10^6$ S/m, thermal conductivity = 6.7 W/(m·K), heat capacity = 526.3 J/(kg·K), density = 4430 kg/m³.

to those at the tissue level, and (b) the adopted filamentary approach to the MBS model does not take into account the thermal properties of the alloy, since the thermal problem is solved only at the tissue level. The usual choice material for MBS, the superelastic austenitic phase of Nitinol, produces a much lower ΔT_{\max} than its martensitic counterpart by virtue of its lower electrical conductivity. It is envisioned that, if the disease progression permits, prospective PDAC patients for magnetic hyperthermia should receive MBSs made of the alloy with the lowest possible electrical conductivity.

4. Conclusions

The use of MBSs as a mean to relieve obstruction in the biliary tree of locally advanced PDAC patients is currently considered as an exclusion criterion in clinical magnetic hyperthermia, and the obtained data from the here proposed electromagnetic model suggest that it should remain as such in some cases. Nevertheless, there are options to improve the current safety prospects for patients with this type of implants. One is the possibility of expanding the use of nonmetallic biodegradable stents [42] that are already widely available from the major vendors, despite the fact that so far MBSs are still those showing the lowest failure and mortality rates [32]. Whenever this replacement is not an option, the use of metals with the lowest electrical conductivity is encouraged to reduce the occurrence of eddy currents as much as possible. We anticipate that this material replacement in MBSs is not as straightforward as in the case of other passive implants, since the shape memory effect must be preserved besides the properties against corrosion.

The bulk of the heat generated in the MBSs upon interaction with the applied field is mainly given by the combination of the wire diameter and the electrical conductivity of the material from which the stent is made. Even for the thinnest wire diameter—which is just below the typical wire diameter in the most widely used MBSs—and a low field intensity, the temperature reached is not negligible.

An added difficulty is the relative orientation of the stent with respect to the applied field. Even small movements of the patient during the treatment can cause significant orientation changes—due to the MBS small size—that may lead to both a completely different heat generation and temperature distribution across the stent. One point that has not been considered here is the benign or malign tissue overgrowth around MBSs, which may change to a variable extent

the heat exchange in the region of interest. This condition directly impacts the treatment safety as it increases the amount of tissue susceptible to thermal damage.

It has to be noted that all the reported results have been obtained considering a continuous field application, but this does not need to be the only possible scenario in clinical magnetic hyperthermia. In those cases where the stent temperature lies at the considered safety limit, the exposure time could be tweaked by introducing a field duty-cycle that takes advantage of the use of pulsed fields, as it has been already tested *in vivo* [6] and it is being tested in the NoCanTher clinical study [31]. In addition, we envision that another way to minimize the extent to which eddy currents happen in MBSs would be the use of coated stents. In our calculations, we have considered a perfect galvanic contact between the different wires that form the stents. If the wires were coated with a thin insulating layer, the galvanic contact would disappear, no loops would be available for the eddy currents and the heating would be virtually nullified.

It also must be noted that the temperature dependence of some physical properties here studied has not been included in the simulations. Thus, the accuracy of the results cannot be ensured when the heating is very large. However, this kind of inaccuracy becomes significant when temperature is beyond the threshold adopted to decide whether the treatment is contraindicated. This means that the results here presented keep their value in terms of ability to identify the situations where the biological tissues surrounding the stent would experience a heating able to damage them irreversibly.

The present work opens up a hitherto unprecedented field of study, i.e., the collateral heating of MBSs in clinical magnetic hyperthermia. Given the wide range of stent geometries in the clinical practice, their physical characteristics (wire diameter, material, etc.) and the possible combinations between them, there is a large number of plausible scenarios, requiring a case-by-case study given the variety of safety implications in terms of unwanted heating. In addition, it is essential to validate the electromagnetic and the thermal models with experimental data, both *in vivo* and in phantoms containing MBSs. This, in turn, brings to light another important shortcoming calling for a swift solution: the lack of accurate data on the physiological response of bile duct under different levels of thermal stress. Therefore, the safety study of MBSs in clinical magnetic hyperthermia should be part of the treatment planning strategy, especially in those cases where the possible occurrence of irreversible thermal damage is not apparent *prima facie*.

Acknowledgments

We are indebted to Drs. Teresa Macarulla, Helena Verdaguer and Raquel Pérez from Vall d'Hebron Institute of Oncology (VHIO) for their support, as well as the Gastrointestinal Tumors Service of the Medical Oncology Service at the University Hospital of Vall d'Hebron for providing the medical images used in this study. We also thank the Systems Unit of the Information Systems Area of the University of Cádiz for computer resources and technical support. Finally, we gratefully acknowledge the support of NVIDIA Corporation through the GPU Grant Program with the donation of the Quadro P6000 GPU used for this research.

Disclosure statement

No potential conflict of interest was reported by the author(s).

Funding

This work has been supported by the NoCanTher project, which has received funding from the European Union's Horizon 2020 research and innovation programme under grant agreement No 685795. The authors acknowledge support from the COST Association through the COST action "MyWAVE" (CA17115). D.O. and I.R.R. acknowledge financial support from the Community of Madrid under Contract No. PEJD-2017-PRE/IND-3663. We acknowledge support under grant PID2020-117544RB-I00, CEX2020-001039-S, RED2018-102626-T and MAT2017-85617-R funded by MCIN/AEI/ 10.13039/501100011033, and grant RYC2018-025253-I funded by MCIN/AEI/ 10.13039/501100011033 and by "FEDER A way of making Europe". The Authors also acknowledge the 18NET05 MATHMET project. This project has received funding from the EMPIR Programme, co-financed by the Participating States and from the European Union's Horizon 2020 Research and Innovation Programme.

ORCID

Oriano Bottauscio  <http://orcid.org/0000-0002-5437-4396>
 Irene Rubia-Rodríguez  <http://orcid.org/0000-0002-0664-5809>
 Alessandro Arduino  <http://orcid.org/0000-0002-4829-5130>
 Luca Zilberti  <http://orcid.org/0000-0002-2382-4710>
 Mario Chiampi  <http://orcid.org/0000-0003-0049-3792>
 Daniel Ortega  <http://orcid.org/0000-0002-7441-8640>

References

- Maier-Hauff K, Rothe R, Scholz R, et al. Intracranial thermotherapy using magnetic nanoparticles combined with external beam radiotherapy: results of a feasibility study on patients with glioblastoma multiforme. *J Neurooncol*. 2007;81(1):53–60.
- Maier-Hauff K, Ulrich F, Nestler D, et al. Efficacy and safety of intratumoral thermotherapy using magnetic iron-oxide nanoparticles combined with external beam radiotherapy on patients with recurrent glioblastoma multiforme. *J Neurooncol*. 2011;103(2):317–324.
- Moss AC, Morris E, Mathuna M. Palliative biliary stents for obstructing pancreatic carcinoma. *Cochrane Database Syst Rev*. 2006;(2):CD004200.
- Dumonceau JM, Heresbach D, Deviere J, European Society of Gastrointestinal Endoscopy, et al. Biliary stents: models and methods for endoscopic stenting. *Endoscopy*. 2011;43(7):617–626.
- Tsiapla A-R, Kalimeri A-A, Maniotis N, et al. Mitigation of magnetic particle hyperthermia side effects by magnetic field controls. *Int J Hyperthermia*. 2021;38(1):511–522.
- Tansi FL, Maduabuchi WO, Hirsch M, et al. Deep-tissue localization of magnetic field hyperthermia using pulse sequencing. *Int J Hyperthermia*. 2021;38(1):743–754.
- Johannsen M, Gneveckow U, Taymoorian K, et al. Morbidity and quality of life during thermotherapy using magnetic nanoparticles in locally recurrent prostate cancer: results of a prospective phase I trial. *Int J Hyperthermia*. 2007;23(3):315–323.
- Rubia-Rodríguez I, Zilberti L, Arduino A, et al. In silico assessment of collateral eddy current heating in biocompatible implants subjected to magnetic hyperthermia treatments. *Int J Hyperthermia*. 2021;38(1):846–861.
- Adibzadeh F, Paulides MM, van Rhoon GC. SAR thresholds for electromagnetic exposure using functional thermal dose limits. *Int J Hyperthermia*. 2018;34(8):1248–1254.
- Ahlbom A, Bergqvist U, Bernhardt JH, et al. Guidelines for limiting exposure to time-varying electric, magnetic, and electromagnetic fields (up to 300 GHz). *Health Phys*. 1998;74(4):494–521.
- Strazzabosco M, Fabris L. Functional anatomy of normal bile ducts. *Anat Rec (Hoboken)*. 2008;291(6):653–660.
- Boulay BR, Parepally M. Managing malignant biliary obstruction in pancreas cancer: choosing the appropriate strategy. *World J Gastroenterol*. 2014;20(28):9345–9353.
- Brelje TC, Sorenson RL. Common Bile Duct 2021. [Available from: <https://www.histologyguide.com/slideview/MHS-261-common-bile-duct/15-slide-1.html>]
- Christ A, Kainz W, Hahn EG, et al. The virtual family—development of surface-based anatomical models of two adults and two children for dosimetric simulations. *Phys Med Biol*. 2010;55(2):N23–N38.
- Gosselin M-C, Neufeld E, Moser H, et al. Development of a new generation of high-resolution anatomical models for medical device evaluation: the virtual population 3.0. *Phys Med Biol*. 2014;59(18):5287–5303.
- Blender 2.79 2017. Available from: <https://www.blender.org/>
- Girard E, Chagnon G, Gremen E, et al. Biomechanical behaviour of human bile duct wall and impact of cadaveric preservation processes. *J Mech Behav Biomed Mater*. 2019;98:291–300.
- Testoni PA, Mariani A, Mangiavillano B, et al. Main pancreatic duct, common bile duct and sphincter of Oddi structure visualized by optical coherence tomography: an ex vivo study compared with histology. *Dig Liver Dis*. 2006;38(6):409–414.
- Mahmud MS, May GR, Kamal MM, et al. Imaging pancreatobiliary ductal system with optical coherence tomography: a review. *World J Gastrointest Endosc*. 2013;5(11):540–550.
- Bonsignore C. Open stent design. *NDC*. 2011;47533:20–47.
- Foundation II. Tissue Properties Database V4. 0. 2018.
- Ren F, Li Q, Gao X, et al. Electrical and thermal analyses of catheter-based irreversible electroporation of digestive tract. *Int J Hyperthermia*. 2019;36(1):853–866.
- Available from: <https://matthey.com/en/products-and-markets/other-markets/medical-components/resource-library/nitinol-technical-properties>
- Available from: <http://www.matweb.com/search/DataSheet.aspx?MatGUID=9bd90091755740648e2afa5cdb9fb09b&ckck=1>
- Laakso I, Hirata A, editors. Improving the computational speed and reducing the staircasing error for simulations of human exposure to low frequency magnetic fields. In International symposium on electromagnetic Compatibility – EMC Europe, 17–21 Sept. 2012.
- Barz C, Petters M, Dorsz A, et al. Possible interactions between stent and electromagnetic field. *Sci Tech Innov*. 2018;3(2):48–51.
- Bottauscio O, Arduino A, Chiampi M, et al. Efficient modelling of implanted medical devices with metallic filamentary loops exposed to low or medium frequency magnetic fields. *Computer Methods and Programs in Biomedicine*. 2022. Available at SSRN: <https://ssrn.com/abstract=4149703>.
- Boyer JL. Bile formation and secretion. *Compr Physiol*. 2013;3(3):1035–1078.
- Boyer JL, Soroka CJ. Bile formation and secretion: an update. *J Hepatol*. 2021;75(1):190–201.
- Johannsen M, Gneveckow U, Thiesen B, et al. Thermotherapy of prostate cancer using magnetic nanoparticles: feasibility, imaging,

- and three-dimensional temperature distribution. *Eur Urol.* **2007**; 52(6):1653–1661.
- [31] Clinical Trial: "Clinical feasibility study of the intratumoral injection of magnetic nanoparticles associated with the treatment of hyperthermia in locally advanced pancreatic cancer for magnetic hyperthermia of locally advanced pancreatic adenocarcinomas", Spanish Agency of Medicines and Medical Devices (AEMPS). **2022**. 797/20/EC.
- [32] Kozarek R, Baron T, Song H-Y. Self-expandable stents in the gastrointestinal tract. New York (NY): Springer Science & Business Media; **2012**.
- [33] Diller KR, Hayes LJ, Blake GK. Analysis of alternate models for simulating thermal burns. *J Burn Care Rehabil.* **1991**;12(2):177–189.
- [34] Diller KR. Modeling of bioheat transfer processes at high and low temperatures. In: Cho YI, editor. *Advances in heat transfer*, vol. 22. New York (NY): Elsevier; **1992**. p. 157–357.
- [35] Garcia PA, Davalos RV, Miklavcic D. A numerical investigation of the electric and thermal cell kill distributions in electroporation-based therapies in tissue. *PLoS One.* **2014**;9(8):e103083.
- [36] Zmuc J, Gasljevic G, Sersa G, et al. Large liver blood vessels and bile ducts are not damaged by electrochemotherapy with bleomycin in pigs. *Sci Rep.* **2019**;9(1):3649.
- [37] Dollinger M, Zeman F, Niessen C, et al. Bile duct injury after irreversible electroporation of hepatic malignancies: evaluation of MR imaging findings and laboratory values. *J Vasc Interv Radiol.* **2016**;27(1):96–103.
- [38] Narayanan G, Bhatia S, Echenique A, et al. Vessel patency post irreversible electroporation. *Cardiovasc Interv Radiol.* **2014**;37(6):1523–1529.
- [39] McDannold N, Vykhotseva N, Jolesz FA, et al. MRI investigation of the threshold for thermally induced blood–brain barrier disruption and brain tissue damage in the rabbit brain. *Magn Reson Med.* **2004**;51(5):913–923.
- [40] Hall JE, Hall ME. *Guyton and hall textbook of medical physiology*. New York (NY): Elsevier Health Sciences; **2020**.
- [41] Ko CW, Lee SP. Epidemiology and natural history of common bile duct stones and prediction of disease. *Gastrointest Endosc.* **2002**; 56(6):S165–S169.
- [42] Song G, Zhao HQ, Liu Q, et al. A review on biodegradable biliary stents: materials and future trends. *Bioact Mater.* **2022**;17: 488–495.

Appendix: Governing electromagnetic equations

The following electromagnetic equation, expressed in terms of the electric scalar potential Φ , is considered within the voxelized domain Ω (human body):

$$\nabla \cdot (\tilde{\sigma} \nabla \Phi) = i\omega \nabla \cdot (\tilde{\sigma} (\mathbf{A}_s + \mathbf{A}_r)). \quad (\text{A.1})$$

In Eq. (A.1) the driving terms are the magnetic vector potential \mathbf{A}_s due to the external coils (field applicator), having angular frequency ω , and the reaction magnetic vector potential \mathbf{A}_r due to the currents (unknowns) induced in the stent wires. $\tilde{\sigma}$ is the complex electrical conductivity of tissues.

The currents induced in the body are confined within the body itself, leading to the following boundary condition on $\partial\Omega$:

$$\nabla \Phi \cdot \mathbf{n} = i\omega (\mathbf{A}_s + \mathbf{A}_r) \cdot \mathbf{n}, \quad (\text{A.2})$$

being \mathbf{n} the unit vector normal to the boundary $\partial\Omega$.

The unknown current densities \mathbf{J}_w flowing in the stent wires are determined approximating the stent wires to an electrical network. The fundamental loop currents of the electrical network were identified through a tree/co-tree decomposition. For the j th fundamental loop \mathfrak{J}_j , the following equation holds:

$$\oint_{\mathfrak{J}_j} \sigma^{-1} \mathbf{J}_w \cdot d\mathbf{l} = -i\omega \oint_{\mathfrak{J}_j} (\mathbf{A}_s + \mathbf{A}_r) \cdot d\mathbf{l}. \quad (\text{A.3})$$

where σ is the electrical conductivity of the wires.

The solution of (A.1) and (A.3) allows the determination of the power dissipated in each branch of the circuit and consequently the one dissipated in the biological tissues, used as input for the successive thermal problem. Computational details of this approach based on filamentary elements can be found in [7].